Journal of Alloys and Compounds 621 (2015) 116–120

Contents lists available at ScienceDirect

Journal of Alloys and Compounds

journal homepage: www.elsevier.com/locate/jalcom

Strength of tungsten triboride under pressure up to 86 GPa from radial X-ray diffraction

Lun Xiong [a,*], Jing Liu [a,*], Ligang Bai [a], Chuanlong Lin [a], Duanwei He [b], Xinxin Zhang [c], Jung-Fu Lin [d]

[a] Institute of High Energy Physics, Chinese Academy of Sciences, Beijing 100049, PR China
[b] Institute of Atomic and Molecular Physics, Sichun University, Chengdu 610065, PR China
[c] State Key Lab of Superhard Materials, Jilin University, Changchun 130012, PR China
[d] Department of Geological Sciences, Jackson School of Geosciences, The University of Texas at Austin, TX 78712, USA

A R T I C L E I N F O

Article history:
Received 30 July 2014
Received in revised form 6 September 2014
Accepted 8 September 2014
Available online 16 September 2014

Keywords:
Tungsten triboride
High pressure
Strength
Radial X-ray diffraction
Diamond anvil cell

A B S T R A C T

The strength of tungsten triboride (WB_3) was determined under nonhydrostatic compression up to 86 GPa using an angle-dispersive radial X-ray diffraction technique in a diamond-anvil cell (DAC). Analyze of diffraction data using lattice strain theory indicate that the ratio of differential stress to shear modulus (t/G) changes from 0.004 at ambient conditions to 0.078 at 86 GPa. Together with theoretical results on the high-pressure shear modulus, our results here show that WB_3 under uniaxial compression can support a differential stress of 26 GPa when it starts to yield to the plastic deformation at 40 GPa. The yield strength of WB_3 increases with increasing pressure, reaching a maximum value of 30 GPa at 77 GPa. By comparison, we find that the high-pressure strength of WB_3 is comparable to those of c-BC_2N, B_6O, and γ-Si_3N_4.

1. Introduction

Many experimental and theoretical studies on boron-tungsten system (WB_x) have suggested that tungsten tetraboride (WB_4) is potentially a superhard material [1,2]. Gu et al. [1] synthesized the compounds formed by transition metals (TMs) and B, and measured their Vickers hardness (Hv) by microindentation tests. The obtained hardness values of WB_4 are 46.2(1.2) GPa and 31.8(1.2) GPa under applied loads of 0.49 N and 4.9 N, respectively. Subsequently, Wang et al. [2] calculated the hardness values of WB_4 to be 41.1–42.2 GPa, consistent with Gu et al. [1], and they [2] pointed out that WB_4 has an ultra-low compressibility with the bulk modulus between 292.7–324.3 GPa. The early works suggested that WB_4 is a potential superhard material and has an ultra-low compressibility. Successively, Mohammadi et al. [3] also measured the hardness by microindentation method as 43.3(2.9) GPa and 28.1(1.4) GPa under an applied load of 0.49 N and 4.9 N, respectively, and reported a bulk modulus $K_0 = 339(3)$ GPa at ambient conditions, for WB_4 from high-pressure X-ray diffraction (XRD) up to 30 GPa in a DAC with neon as the pressure medium. Liu et al. [4] performed the high-pressure XRD of WB_4 up to 51 GPa with silicone oil as the pressure medium and obtained $K_0 = 325(9)$ GPa with $K_0' = 5.1(0.6)$. Both K_0 and K_0' are defined in the Birch-Monaghan equation of state (EoS). Xie et al. [5] measured the compression behavior of WB_4 with neon as the pressure medium up to 59 GPa and obtained $K_0 = 369(9)$ GPa with $K_0' = 1.2(0.5)$ by fitting the data at pressures lower than 42 GPa. Xiong et al. [6] reported a bulk modulus $K_0 = 319(5)$ GPa with $K_0' = 4.1(0.2)$ at $\psi = 54.7°$ by fitting the radial X-ray diffraction (RXD) nonhydrostatic compression data to 86 GPa.

However, subsequent theoretical studies indicated that the structure of WB_4 is unstable and the previously believed WB_4 is in fact WB_3 [7,8]. Liang et al. [7] evaluated the structure stability of WB_x from first principles, and questioned the stability of WB_4 for the first time. They reported that long-believed WB_4 is actually WB_3 because their Gibbs energy shows that the WB_3 is thermodynamically stable and WB_4 is not. Subsequently, Liang et al. [9] reported that WB_3 is superhard due to its three-dimensional covalent network consisting of boron honeycomb planes interconnected with strong zigzag W–B bonds. Liang et al. [9] calculated the Vickers hardness of WB_4 (16.8 GPa) and WB_3 (43.1 GPa) using the linear correlation existing between the Vickers hardness and shear modulus for many of the known hard materials and superhard materials. They obtained the Vickers hardness of WB_4 (6.8 GPa) and WB_3 (39.4 GPa) from theoretical calculation using Chen's model of hardness. The hardness of WB_4 (16.8 GPa, 6.8 GPa) is ~39% of WB_3 (43.1 GPa, 39.4 GPa). Zhang et al. [8]

* Corresponding authors.
E-mail addresses: xionglun@ihep.ac.cn (L. Xiong), liuj@ihep.ac.cn (J. Liu).

http://dx.doi.org/10.1016/j.jallcom.2014.09.076
0925-8388/© 2014 Published by Elsevier B.V.

compared experimental and theoretically calculated XRD patterns between WB_4 and WB_3, along with the thermodynamic, mechanical, and phonon instabilities of WB_4 using density functional theory. They denoted that WB_4 with a three-dimensional boron network is identified as WB_3 with two-dimensional boron nets. In addition, they suggested that WB_3 may not be an intrinsically superhard material due to its much lower ideal shear strengths compared with the superhard material of *c*-BN. Zang et al. [10] calculated the stress–strain relation and the ideal strength of WB_3 using the first-principles, leading the authors to conclude that the Vickers hardness of WB_3 should be well below that of ReB_2, which implies that WB_3 cannot be a superhard material. Li et al. [13] examined tungsten borides using a recently developed global structural optimization approach and identified the thermodynamically stable structures. They reported that comparison of experimental and simulated X-ray diffraction patterns leads to the identification of $P6_3/mmc$-4*u* WB_3, while R-3m-6*u* WB_3 is thermodynamically stable and thus viable for experimental synthesis. These studies indicate that WB_4 is unstable and leaves the issue of whether or not WB_3 is a superhard material under debate.

Despite several theoretical calculations for WB_3, there are no direct experimental measurements. There are different opinions regarding whether WB_3 is a superhard material. Previous studies have shown that the hardness of materials has some relationship with strength which reflects the contributions of both plastic and elastic deformation. In this study, we have investigated the strength of WB_3 to 86 GPa under nonhydrostatic compression using radial X-ray diffraction (RXD) in diamond-anvil cell.

2. Experimental details

The WB_3 powder was synthesized in a DS6 * 8MN cubic press [14] at high-pressure and temperature conditions. The synthesized WB_3 sample possesses an average grain size of 0.5–1 μm determined via scanning electron microscopy (SEM). Fig. 1 displays the XRD pattern of the synthesized WB_3 and simulated patterns for WB_4 and WB_3 reported by Zhang et al. [8]. It can be seen that the XRD pattern of synthesized sample matches much better with that of the simulated WB_3 from Zhang et al. [8]. The measured XRD pattern shows the highly crystalline and pure phase. At ambient conditions, the synthesized WB_3 has a hexagonal structure (space group $P6_3/mmc$, see Fig. 2) with lattice parameters a = 5.199(0.001) Å and c = 6.347(0.001) Å.

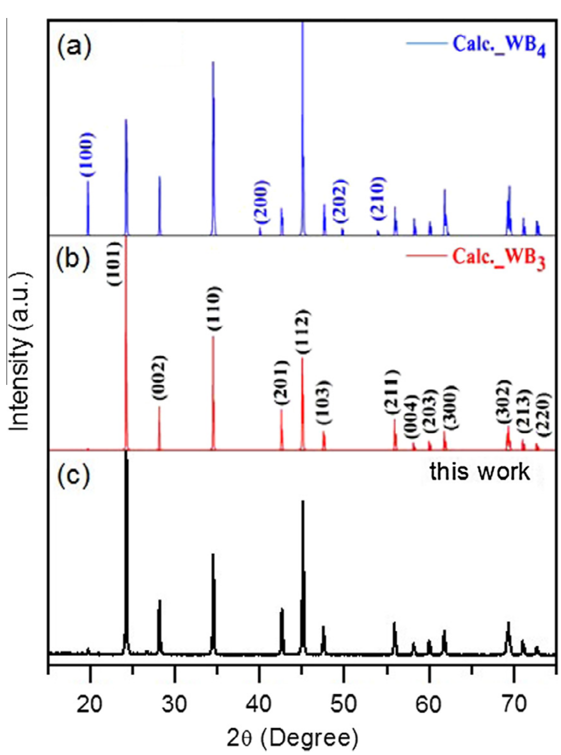

Fig. 1. Representative powder X-ray diffraction pattern for tungsten triboride (WB_3) at ambient conditions (λ = 1.5406 Å). The XRD pattern is in agreement with Zhang et al. [8]. The corresponding Miller indices are noted for each peak. X-ray wavelength λ = 1.5406 Å.

A twofold panoramic DAC with a pair of beveled diamond anvils (150 μm culet diameter) was used to exert uniaxial compression on both the WB_3 sample and Mo standard in the RXD measurements. A beryllium gasket was pre-indented to ~25-μm thickness at ~20 GPa and a hole of 50-μm-diameter was drilled in the center of the preindented area for use as a sample chamber. Special attention was paid to make sure that the sample hole was well centered with respect to the anvil culet. The WB_3 sample was loaded into the gasket hole and a piece of Mo flake with a diameter of ~20 μm was placed on top within 5 μm of the sample center serving as a pressure standard [15] as well as the positioning reference for X-ray diffraction. No pressure-transmitting medium was used to ensure maximum nonhydrostatic stresses. By design, the DAC was tilted at an angle of 28° to minimize the contribution of Be diffraction to the sample patterns [16]. Angle-dispersive radial X-ray diffraction experiments were performed at the 4W2 beam line of Beijing Synchrotron Radiation Facility (BSRF), Chinese Academy of Sciences. A Si(1 1 1) monochromator was used to tune the synchrotron source to a wavelength of 0.6199 Å, and the incident monochromatic X-ray beam was focused by a pair of Kirkpatrick-Baez mirrors to an approximately 26(vertical) × 8(horizontal) μm^2 spot of full width at half maximum (FWHM) and directed through the Be gasket and the sample. Two-dimensional diffraction patterns were collected by a Mar345 image plate detector and analyzed with the program Fit2D [17]. The sample-to-detector distance and orientation of the detector were calibrated by a CeO_2 standard. At each pressure, the RXD pattern was collected typically for 15–20 min after about 30 min of stress relaxation.

3. Theory

The radial X-ray diffraction data was analyzed using the lattice strain theory developed by Singh and co-workers [18,19]. According to the lattice strain theory, the measured *d*-spacing $d_m(hkl)$ is a function of the azimuthal angle ψ between the DAC loading axis and the diffraction plane normal (hkl), and can be calculated using the relation as

$$d_m(hkl) = d_p(hkl)[1 + (1 - 3\cos^2\psi)Q(hkl)] \tag{1}$$

where $d_m(hkl)$ is the measured *d*-spacing, $d_p(hkl)$ is the *d*-spacing under the equivalent hydrostatic pressure, and $Q(hkl)$ is the orientation dependent lattice strain.

Under isostress conditions (the Reuss limit), the differential stress, t, can be expressed as

$$t = 6G\langle Q(hkl)\rangle \tag{2}$$

where $\langle Q(hkl)\rangle$ represents the Q value averaged over all observed reflections of $Q(hkl)$, and G is the aggregate shear modulus of the polycrystalline sample. The pressure dependence of G can be obtained from extrapolation of ultrasonic or theoretically calculated single-crystal elastic constants. If the differential stress t has reached the limiting value of yield strength at high pressures when

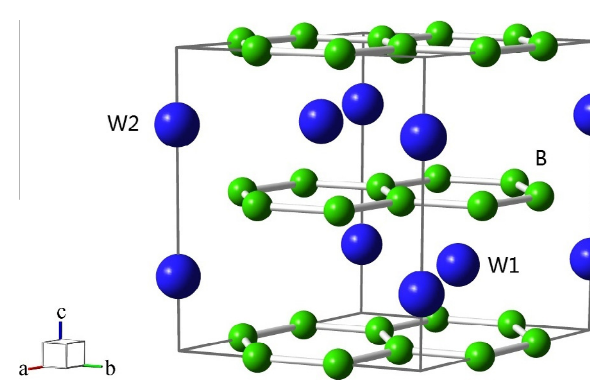

Fig. 2. Crystal structure of WB_3.

materials start to deform plastically, $6\langle Q(hkl)\rangle = t/G$ will reflect the ratio of yield strength to shear modulus. In addition, this ratio might be a good qualitative indicator of hardness as it reflects the contributions of both plastic and elastic deformation [20].

Eq. (1) indicates that the $d_m(hkl)$ vs $(1–3\cos^2\psi)$ plot is a straight line for given $d_p(hkl)Q(hkl)$, and its slope, $d_p(hkl)Q(hkl)$, is directly related to $t/G = 6\langle Q(hkl)\rangle$. $d_p(hkl)$ is normally at $\psi = 54.7°$. With additional, independent constraints on the high-pressure shear modulus, the differential stress or yield strength at high pressure can be determined.

For the conventional RXD experiments, the incident X-ray beam is perpendicular to the compression axis and passes through a Be gasket which contributes intense diffraction lines to the sample patterns. Thus, we can tilt the DAC to an angle of α between the compression axis and the incident X-ray to minimize the Be contribution to the sample patterns ($\alpha = 28°$) [16]. In this geometry, ψ in Eq. (1) can be rewritten as [21]

$$\cos\psi_{hkl} = \sin\alpha\cos\delta\cos\theta_{hkl} + \cos\alpha\sin\theta_{hkl} \quad (3)$$

where θ is the diffraction angle and δ is the azimuthal angle in the plane of the detector.

4. Results and discussion

The RXD diffraction patterns are integrated over each azimuthal sector with a 5° interval using Fit2D [17] for data analyzes. The program Multifit 4.2 is used to perform macro decomposition of the 2D diffraction images into azimuthal slices within Fit2D [17], yielding one-dimensional plots of X-ray intensity as a function of $2\theta t$, as well as peak positions, intensities, and FWHM of the diffraction peaks. To determine the variation of the diffraction peak positions with δ, we integrated the diffraction patterns with segments of 5° in the azimuth angle, in the range of 180–270°, and fit peak positions. RXD spectra of WB_3 were collected up to an equivalent pressure of 86 GPa, where pressures were derived from the EoS of Mo [15] with the unit cell volume obtained from $d_p(110)$ of Mo at ψ=54.7°.

The plots of d-spacing as a function of $1–3\cos^2\psi$ for selected diffraction peaks of WB_3 at 45 GPa are shown in Fig. 3. As expected from the lattice strain theory [18,19], d-spacing for all diffraction peaks shows a linear relationship with $1–3\cos^2\psi$. The (101) peak of WB_3 exhibits a slope that is about twice as great as that of the (201) peak, indicating that the (201) peak is more sensitive to nonhydrostatic stresses compared to the (101) peak.

According to Eq. (1), the orientation dependent lattice strain $Q(hkl)$ can be derived from the slope of the linear relationship between the observed d-spacing and $1–3\cos^2\psi$. The ratio of t/G was obtained from the averaged value of $Q(hkl)$ over all observed reflections. Fig. 4 displays $t(hkl)/G$ as a function of WB_3 pressure. The large variations for different lattice planes are due to differences in stress levels for different lattice orientations and are an indication of high elastic anisotropy in the material. $t(002)/G$ is the largest at nearly double the smallest ratio, $t(101)/G$. For WB_3, the ratio of t/G ranges from 0.004 to 0.076 at pressures of 1–86 GPa with an average value of 0.051. High t/G values of WB_3 indicate that WB_3 may serve as a structural template for designing superhard materials. The ratio of t/G remains almost unchanged above ~40 GPa, indicating that WB_3 undergoes plastic deformation and t/G reaches its limiting value of 0.076 at this pressure. This ratio might be a good qualitative indicator of hardness as it reflects the contributions of both plastic and elastic deformation. In addition, the increase in t/G WB_3 levels off after ~77 GPa, suggesting that the local deviatoric stress is partially relaxed.

Together with the results of first-principles calculation on high-pressure shear modulus (Fig. 5), we obtained the differential stress at each pressure step as t=6$G\langle Q(hkl)\rangle$. Fig. 6 compares differential stresses obtained for several superhard materials (c-BC_2N [22], B_6O [23], γ-Si_3N_4 [24]) from RXD in the DAC. It can be seen that, the differential stress, t, increases slowly above ~40 GPa, indicating that WB_3 begins to experience macro yield with plastic deformation as t reaches its limited value (yield strength) of 25.5 GPa at this pressure. In addition, after ~77 GPa, the differential stress begins to level off, and similar behaviors were observed for c-BC_2N [22].

At ~77 GPa, differential stress as high as ~30 GPa is supported by WB_3. For comparison, a differential stress of ~38 GPa is supported by c-BC_2N [22] at ~66 GPa, B_6O [23] supports a maximum differential stress of ~30 GPa at a confining pressure of 65 GPa, and γ-Si_3N_4 [24] reaches a maximum differential stress of 23 GPa at a pressure of 68 GPa. The differential stress of WB_3 is very large

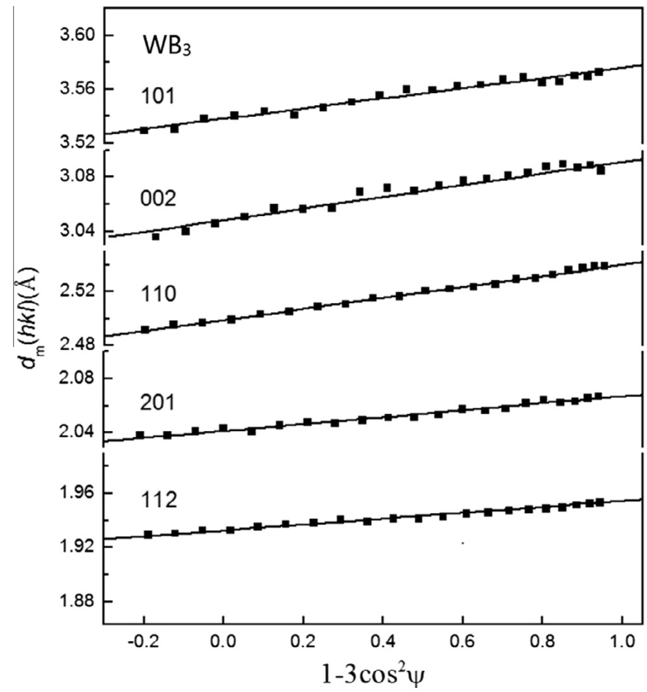

Fig. 3. d Spacings vs $1–3\cos^2\psi$ for selected diffraction peaks of WB_3 at 45 GPa. The solid lines are least-squares linear fits to the data. The pressures are determined from the Mo(110) peak at $\psi = 54.7°$.

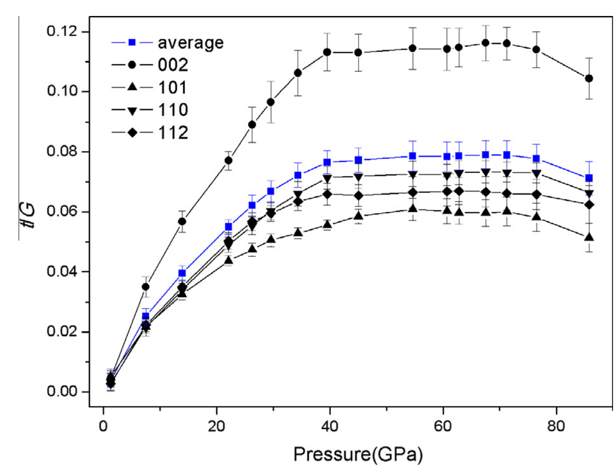

Fig. 4. Ratio of differential stress to shear modulus (t/G) as a function of pressure for WB_3. The errors are estimated from the variations of $d(hkl)$ vs $1–3\cos^2\psi$.

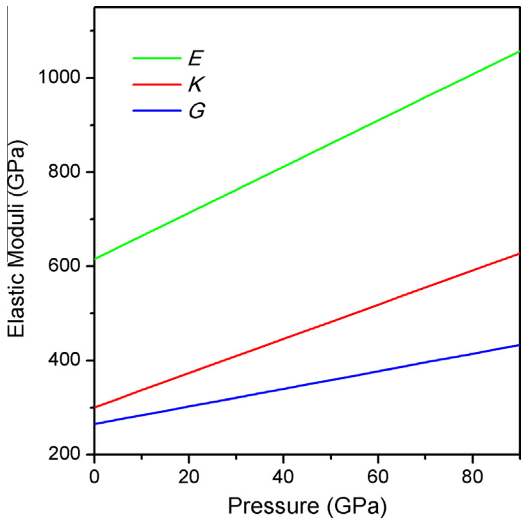

Fig. 5. Linear fits to the isotropic elastic moduli of WB_3 as a function of pressure.

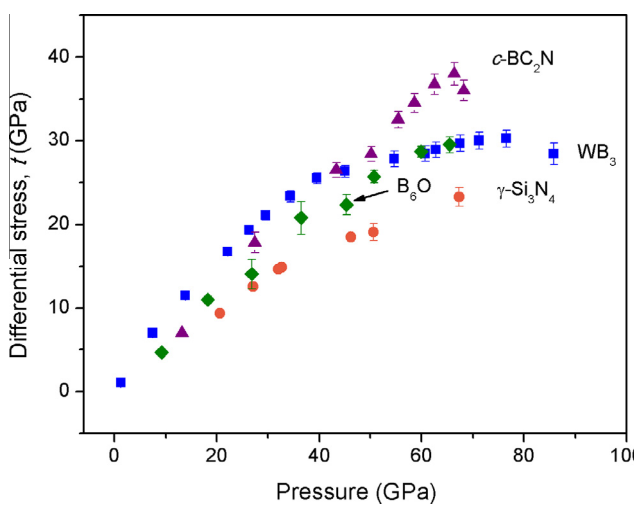

Fig. 6. Differential stress as a function of pressure for WB_3, *c*-BC_2N, B_6O, and γ-Si_3N_4.

due to its large t/G and large shear moduli. It can be seen that, the maximum differential stress in the pressure range studied of WB_3 is close to that of B_6O [23], which is much larger than that of γ-Si_3N_4 [24], but lower than that of *c*-BC_2N [22].

The differential stress of WB_3 is even "higher" than that of *c*-BC_2N, B_6O, and γ-Si_3N_4 below 40 GPa, and it seems that WB_3 is "harder" than these materials. However, the Vickers hardness should consider the maximum differential stress before yield [20], as well as grain size [25]. WB_3 experiences macro yield with plastic deformation at ~40 GPa and sustains a differential stress of ~25.5 GPa. For comparison, *c*-BC_2N begins to yield at a pressure of ~66 GPa with a maximum differential stress of ~38 GPa, and B_6O started to yield at nonhydrostatic compression of ~65 GPa and differential stress reaches its limiting yield strength value of 29.5 GPa. For γ-Si_3N_4, the yield point is ~67 GPa with a yield strength of ~23 GPa. In addition, the strength of polycrystalline materials is also known to increase with decreasing grain size, and grain-size effects on high-pressure strength have been documented in previous RXD experiments [25]. Hence, grain-size effects on high-pressure strength should also be taken into account when comparing WB_3 (microcrystalline), *c*-BC_2N [22] (nanocrystalline), B_6O (microcrystalline) [23] and γ-Si_3N_4 (nanocrystalline) [24]. The results probably indicate that the Vickers hardness of WB_3 is lower than that of *c*-BC_2N (~70 GPa [29]), B_6O, (45 GPa [25]), and γ-Si_3N_4 (35 GPa [26] and 43 GPa [27,28]).

Liang et al. [9] obtained a Vickers hardness of 39.4 GPa for WB_3 from theory calculation using Chen's model of hardness [15] and 43.1 GPa using the correlation [31] existing between the Vickers hardness and shear modulus. However, Zhang et al. [8] demonstrate that WB_3 cannot be intrinsically superhard because of its much lower ideal strengths compared to *c*-BN. And Zang et al. [10] argue that the Vickers hardness of WB_3 should be well below that of ReB_2 (30.1 GPa [11], 26.6 GPa [1], and 18.4 GPa [12]) as calculating the stress–strain relation and the ideal indentation strength from first-principles shows that the calculated ideal indentation strength of WB_3 is considerably lower than that of ReB_2 via calculating the stress–strain relation and the ideal strength.

5. Conclusion

We have examined the strength of WB_3 in a diamond anvil cell under nonhydrostatic compression up to 86 GPa at room temperature using radial X-ray diffraction together with the lattice strain theory. The differential stress of WB_3 increases with pressure from 0.4% of the shear modulus at 1 GPa to 7.8% at 77 GPa. Given the theoretically calculated values for the shear modulus at high pressures, the supported differential stress ranges from 1 GPa at 1 GPa to 30 GPa at 77 GPa. The change of t with pressure indicates that WB_3 starts to yield with plastic deformation and t reaches 26 GPa at a nonhydrostatic compression of ~40 GPa. The increase in t with pressure reaches a maximum value of 30 GPa at ~77 GPa. The differential stresses of WB_3 are comparable to those of several reported superhard materials (c-BC_2N, B_6O, γ-Si_3N_4).

Acknowledgments

The authors thank Jiaqian Qin and Shuai Yin for synthesizing WB_3 sample, Guangtao Liu and Haofei Zhao for first-principles calculations on high-pressure shear moduli of WB_3, Haini Dong for helpful discussion. Xiaodong Li for technical assistance, Rui Li, Yanming Ma, and Sheng-nian Luofor article revision. Financial supports from the National Natural Science Foundation of China (Nos. 10875142, 11027405, and 10976018), and the National Basic Research Program of China (No. 2011CB808200) are gratefully acknowledged. This work was performed at 4W2 beam line of Beijing Synchrotron Radiation Facility (BSRF), which is supported by Chinese Academy of Sciences under Grant Nos. KJCX2-SWN03 and KJCX2-SW-N20. J.F.L. acknowledges financial support from Energy Frontier Research in Extreme Environments (EFree) Center and NSF Earth Sciences (EAR-0838221).

References

[1] Q.F. Gu, G. Krauss, W. Steurer, Adv. Mater. 20 (2008) 3620–3626.
[2] M. Wang, Y.W. Li, T. Cui, Y.M. Ma, G.T. Zou, Appl. Phys. Lett. 93 (2008) (1907) 101905–101910.
[3] R. Mohammadi, A.T. Lech, M. Xie, B.E. Weaver, M.T. Yeung, S.H. Tolbert, R.B. Kaner, Proc. Natl. Acad. Sci. 108 (2011) 10958–10962.
[4] C.J. Liu, F. Peng, N. Tan, J. Liu, F.J. Li, J.Q. Qin, J.H. Wang, Q.M. Wang, D.W. He, High Press. Res. 31 (2011) 275–282.
[5] M. Xie, R. Mohammadi, Z. Mao, M.M. Armentrout, A. Kavner, R.B. Kaner, S.H. Tolbert, Phys. Rev. B 85 (2012) 064118–064125.
[6] L. Xiong, J. Liu, L.G. Bai, Y.C. Li, C.L. Lin, D.W. He, F. Peng, J.F. Lin, J. Appl. Phys. 113 (2013) 033507–033511.
[7] Y.C. Liang, X. Yuan, W.Q. Zhang, Phys. Rev. B 83 (2011) 220102(R)–220105(R).
[8] R.F. Zhang, D. Legut, Z.J. Lin, Y.S. Zhao, H.K. Mao, S. Veprek, Phys. Rev. Lett. 108 (2012) 255502–255506.
[9] Y.C. Liang, Z. Fu, X. Yuan, S.M. Wang, Z. Zhong, W.Q. Zhang, EPL (Europhys. Lett.) 98 (2012) 66004–66009.
[10] C.P. Zang, H. Sun, C.F. Chen, Phys. Rev. B 86 (2012) 180101(R)–180105(R).

[11] H.Y. Chung, M.B. Weinberger, J.B. Levine, A. Kavner, J.M. Yang, S.H. Tolbert, R.B. Kaner, Science 316 (2007) 436–439.
[12] J.Q. Qin, D.W. He, J.H. Wang, L.M. Fang, L. Lei, Y.J. Li, J.A. Hu, Z.L. Kou, Y. Bi, Adv. Mater. 20 (2008) 4780–4783.
[13] Q. Li, D. Zhou, W.T. Zheng, Y.M. Ma, C.F. Chen, Phys. Rev. Lett. 110 (2013) 136403–136407.
[14] H. Ma, D.W. He, L. Lei, S.M. Wang, Y. Chen, H.K. Wang, J. Alloys Comp. 509 (2011) L124–L127.
[15] R.S. Hixson, J.N. Fritz, J. Appl. Phys. 71 (1992) 1721–1728.
[16] A.K. Singh, J. Phys. Chem. Solids 65 (2004) 1589–1596.
[17] A.P. Hammersley, S.O. Svensson, M. Hanfland, A.N. Fitch, D. Häusermann, High Press. Res. 14 (1996) 235–248.
[18] A.K. Singh, J. Appl. Phys. 73 (1993) 4278–4286.
[19] A.K. Singh, C. Balasingh, J. Appl. Phys. 75 (1994) 4956–4962.
[20] M. Fujikane, M. Leszczynski, S. Nagao, T. Nakayama, S. Yamanaka, K. Niihara, R. Nowak, J. Alloys Comp. 450 (2008) 405–411.
[21] S. Merkel, H.R. Wenk, J.F. Shu, G.Y. Shen, P. Gillet, H.K. Mao, R.J. Hemley, J. Geophys. Res. 107 (2002) 2271–2287.
[22] H.N. Dong, D.W. He, T.S. Duffy, Y.S. Zhao, Phys. Rev. B 79 (2009) 014105–014110.
[23] D.W. He, S.R. Shieh, T.S. Duffy, Phys. Rev. B 70 (2004) 184121–184129.
[24] B. Kiefer, S.R. Shieh, T.S. Duffy, T. Sekine, Phys. Rev. B 72 (2005) 014102–014111.
[25] J.R. Ryu, K. Moon, K.S. Lee, J. Alloys Comp. 296 (2000) 157–165.
[26] D.W. He, Y.S. Zhao, L. Daemen, J. Qian, T.D. Shen, T.W. Zerda, Appl. Phys. Lett. 81 (2002) 643–645..
[27] J.Z. Jiang, F. Kragh, D.J. Frost, K. Ståhl, H. Lindelov, J. Phys.: Condens. Matter 13 (2001) L515–L520.
[28] I. Tanaka, F. Oba, T. Sekine, E. Ito, A. Kubo, K. Tatsumi, H. Adachi, T. Yamamoto, J. Mater. Res. 17 (2002) 731–733.
[29] A. Zerr, M. Kempf, M. Schwarz, E. Kroke, M. Goken, R. Riedel, J. Am. Ceram. Soc. 85 (2002) 86–90.
[31] D.M. Teter, MRS Bull. 23 (1998) 22–27.

Further reading

[30] Y. Zhao, D.W. He, L.L. Daemen, T.D. Shen, R.B. Schwarz, Y. Zhu, D.L. Bish, J. Huang, J. Zhang, G. Shen, J. Qian, T.W. Zerda, J. Mater. Res. 17 (2002) 3139–3145.